ELSEVIER

Thermochimica Acta 304/305 (1997) 335–346

thermochimica acta

Modulated differential scanning calorimetry: XI. A characterisation method for interpenetrating polymer networks

M. Song[a], D.J. Hourston[b,*], H.M. Pollock[a], F.U. Schäfer[b], A. Hammiche[a]

[a] *School of Physics and Chemistry, Lancaster University, Lancaster LA1 4YB, UK*
[b] *IPTME, Loughborough University, Loughborough LE11 3TU, UK*

Received 13 July 1996; accepted 24 February 1997

Abstract

Quantitative analysis of the differential of heat capacity with temperature, dC'_p/dt, signal from modulated-temperature differential scanning calorimetry (M-TDSC) allows the extent of phase mixing to be calculated for interpenetrating polymer networks (IPNs). A new characterisation method for interpenetrating polymer networks is proposed in which the dC'_p/dT signal was used to analyse phase structure and composition. It is believed that the dC'_p/dT with temperature signal will become a useful tool and a powerful complement to solid-state NMR, scattering and direct nonradiative energy-transfer methods for analysing the morphology of IPNs. © 1997 Elsevier Science B.V.

Keywords: Glass transition; Heat capacity; Interpenetrating polymer network; Modulated-temperature DSC; Polymer characterisation

1. Introduction

Polymers continue to play an ever-increasing role in the modern world. As a result of the increased volume and variety of materials currently available, and the diversity of their application, characterisation has become an essential requirement of industrial and academic laboratories involved with polymeric materials. These requirements may come from polymer specialists, engaged in the design and synthesis of new materials, who require a detailed understanding of the relationship between the precise molecular architecture and the properties of the polymer in order to improve its capabilities and range of applications.

Optical and electron microscopes are useful tools to characterise the morphology of polymeric materials, especially multi-phase materials [1]. Scattering techniques are generally superior as far as the quantification of microstructure is concerned. Interfacial thickness, which is an important structure parameter for multi-phase materials, can be studied by means of scattering techniques [2]. The methods involve either the best fitting of experimental scattering profiles with theoretical profiles [3] or analyses of the systematic deviation of small-angle scattering curve at the large-angle tail from the Porod rule due to finite interfacial thickness [4–6]. The latter method is useful to determine the narrow interfacial thickness, but is not appropriate for systems with a broad interfacial region that invokes a significant reduction of the scattered intensity in the angular region where the Porod rule is

*Corresponding author.

PII S0040-6031(97)00124-X

applicable. For systems with a broad interfacial region, the former method is more appropriate than the latter and becomes very powerful, especially when the scattering curves exhibit a number of scattering maxima [3,6]. However, the experimental difficulties of the methods, competing effects and practical applications to multi-phase materials have been discussed fully by a number of authors [7,8].

In studying multi-phase materials, dynamic mechanical data can be modelled by assuming an interfacial profile [9], but this method requires large interface volume fractions and highly ordered systems. Obviously, its application is very limited.

It is difficult to obtain weight or volume fractions of each component in multi-phase polymeric materials by means of aforementioned technique. If a characteristic method, which determines weight fraction and gives information on the concentration distribution in multi-phase polymeric materials, can be found, this would provide very valuable information about heterogeneous polymer systems.

1.1. Theoretical background to M-TDSC analysis in the glass transition region

A differential equation to describe the kinetics of enthalpy (H) relaxation for conventional differential scanning calorimetry (DSC) has been suggested [10].

$$\mathrm{d}\delta/\mathrm{d}t = \Delta C_\mathrm{p} q - \delta/\tau(T,\delta) \tag{1}$$

In this equation, $\delta(= H - H_\infty)$ is the excess enthalpy relative to the equilibrium value (H_∞), ΔC_p the difference between the liquid (C_p^l) and glassy (C_p^g) specific heat capacities, q the heating rate and t the time.

The single relaxation time τ depends [10] upon both T and δ, according to Eq. (2).

$$\tau = \tau_\mathrm{g}\exp\left[-\theta(T - T_\mathrm{g})\right]\exp\left[-(1-x)\theta\delta/\Delta C_\mathrm{p}\right] \tag{2}$$

Here, τ_g is the relaxation time at equilibrium at the glass temperature T_g, x the nonlinearity parameter ($0 \le x \le 1$), and θ a constant defining the temperature dependence of t. It is obtained by using the following approximation:

$$\theta = \Delta h^*/(RT_\mathrm{g}^2) \tag{3}$$

where Δh^* is an apparent activation energy. Eqs. (1) and (2) define the response of the glass to any prescribed thermal history. For simplicity, the following approximate equation will be used in this paper for the relaxation time τ.

$$\tau = \tau_\mathrm{g}\exp\left[-\theta(T - T_\mathrm{g})\right] \tag{4}$$

The basic principle is to superimpose upon the conventional DSC heating rate a periodically varying temperature modulation. In M-TDSC, this modulation is sinusoidal, giving a time-dependent temperature as follows [11]:

$$T = T_0 + qt + A_\mathrm{T}\sin(\omega t) \tag{5}$$

T_0 is the initial temperature of the DSC scan, A_T the amplitude of temperature modulation, and ω the frequency of modulation.

Using the variable $\eta = \delta + T\Delta C_\mathrm{p}$, Lacey et al. [12] made approximations to Eq. (1), which lead to the following equation [12]:

$$\begin{aligned}\mathrm{d}\eta/\mathrm{d}t &= \exp\left[\Delta h^*/(RT_\mathrm{g}^2)(T - T_\mathrm{g})\right](T\Delta C_\mathrm{p} - \eta)/\tau_\mathrm{g} \\ &= \left[\Delta C_\mathrm{p} qt + A_\mathrm{T}\Delta C_\mathrm{p}\sin(\omega t) - \eta\right] \\ &\quad \times \exp\left[Kqt + KA_\mathrm{T}\sin(\omega t)\right]/\tau_0\end{aligned} \tag{6}$$

$$\tau_0 = \exp\left(\Delta h^*/(RT_\mathrm{g})\right)\tau_\mathrm{g} \tag{7}$$

For M-TDSC, Lacey et al. [12] proposed that $\eta = \langle\eta\rangle + A_\mathrm{T}\mathrm{Re}\{\phi\exp(i\omega t)\}$. $\langle\eta\rangle$ is the underlying part of η and satisfies

$$\mathrm{d}\langle\eta\rangle/\mathrm{d}t = \left[\Delta C_\mathrm{p} qt - \langle\eta\rangle\right]\exp(Kqt)/\tau_0 \tag{8}$$

where ϕ is the 'complex amplitude' [12]:

$$\begin{aligned}i\omega\phi\exp(i\omega t) = \exp(i\omega t)&\left[K(\Delta C_\mathrm{p} qt - \langle\eta\rangle)\right. \\ &\left. + \Delta C_\mathrm{p}\right]\exp(Kqt)/\tau_0 \\ &- \exp(Kqt)/\tau_0\phi\exp(i\omega t)\end{aligned} \tag{9}$$

Then

$$\begin{aligned}\langle\eta\rangle = A\exp\left[-e^{Kqt}/(Kq\tau_0)\right] &+ qt\Delta C_\mathrm{p} \\ &- q\Delta C_\mathrm{p}\exp\left[-e^{Kqt}/(Kq\tau_0)\right]\int_0^t \\ &\times \exp\left[e^{Kqt'}/(Kq\tau_0)\right]\mathrm{d}t'\end{aligned} \tag{10}$$

and

$$\begin{aligned}\phi = i\{&K(\langle\eta\rangle - qt\Delta C_\mathrm{p} - \Delta C_\mathrm{p}]/ \\ &[1 + i\omega t_0\exp(-Kqt)]\end{aligned} \tag{11}$$

For M-TDSC [13],

$$dQ/dt = C_{pt}\,dT/dt + f(t,T) = qC_{pt} + \langle f(t,T)\rangle + \omega A_T C_{pt}\cos(\omega t) + C\sin(\omega t) \quad (12)$$

dQ/dt is the heat flow into the sample, C_{pt} the reversing heat capacity of the sample due to its molecular motions at the heating rate q, $f(t,T)$ is the heat flow arising as a consequence of a kinetically retarded event, $\langle f(t,T)\rangle$ is the average of $f(t,T)$ over the interval of at least one modulation and C is the amplitude of the kinetically retarded response to the temperature modulation.

Consider the complex heat capacity, C_p^*

$$C_p^* = A_{HF}/A_q \quad (13)$$

A_{HF} and A_q are the amplitudes of heat flow and heating rate, respectively.

The complex heat capacity is out of phase with the heating rate, and a real part, C_p', and an imaginary part, C_p'' may be assigned [13]:

$$C_p' = C_p^*\cos\alpha$$
$$C_p'' = C_p^*\sin\alpha \quad (14)$$
$$C_p^* = C_p' - iC_p'' \quad (15)$$

α is the phase angle between heat flow and heating rate.

Also, we have [13]

$$dQ/dt = C_{pt}dT/dt + f(t,T) = qC_{pt} + \langle f(t,T)\rangle + \omega A_T C_{p\omega}\cos(\omega t) + \sin(\omega t) \quad (16)$$

$C_{p\omega}$ is the reversing heat capacity at the frequency ω.

Since $dQ/dt = C_{pg}dT/dt + d\eta/dt$, we have [12]

$$qC_{pt} + \langle f(t,T)\rangle = qC_{pg} + d\langle\eta\rangle/dt \quad (17)$$

and

$$\omega A_T C_{p\omega}\cos(\omega t) + C\sin(\omega t) = [(C_{pg} - \mathrm{Im}\{\phi\}\cos(wt) - \mathrm{Re}\{\phi\}\sin(wt)] \quad (18)$$

'Re' and 'Im' refer to the real and the imaginary parts, respectively.

Assuming $C_p' = A + BT + F(T)$ during the glass transitions, according to Lacey et al. [12], C_p' and C_p'' can be obtained:

$$C_p' = A + BT + \Delta C_p(1 - \exp(-\Delta h^* T/(RT_g^2))/(1 + \omega^2\tau_g^2\exp(-2\Delta h^*/(RT_g^2)(T - T_g))) \quad (19)$$

$$C_p'' = \Delta C_p\omega\tau_g\exp(-\Delta h^*/RT_g^2)(T - T_g)) \times (1 - \exp(-\Delta h^* T/(RT_g^2))/(1 + \omega^2\tau_g^2\exp(-2\Delta h^*/(RT_g^2)(T - T_g))) \quad (20)$$

Figs. 1–3 show the C_p', C_p'' and T_g vs. frequency for polystyrene. For this theoretical analysis, the following parameters were used: $\Delta C_p = 0.3\ \mathrm{J\ g^{-1}\,^{\circ}C^{-1}}$ (from [10]); $\Delta h^* = 300\ \mathrm{kJ\ mol^{-1}}$ (assumed value):

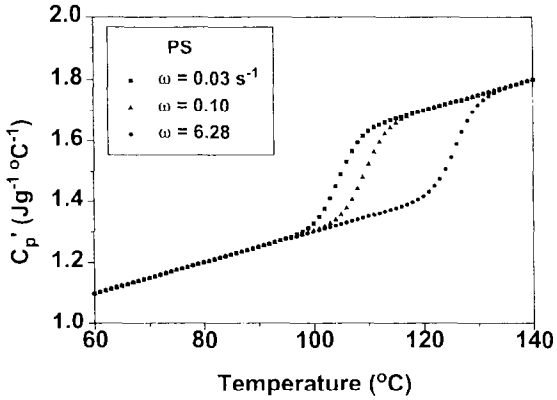

Fig. 1. Theoretical C_p' vs. frequency curves for polystyrene at different frequencies.

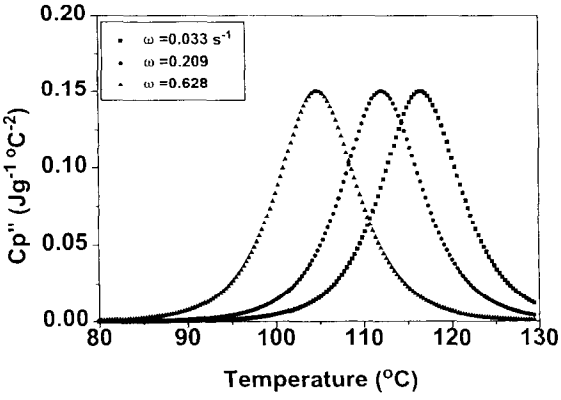

Fig. 2. Theoretical C_p'' vs. temperature curves for polystyrene at different frequencies.

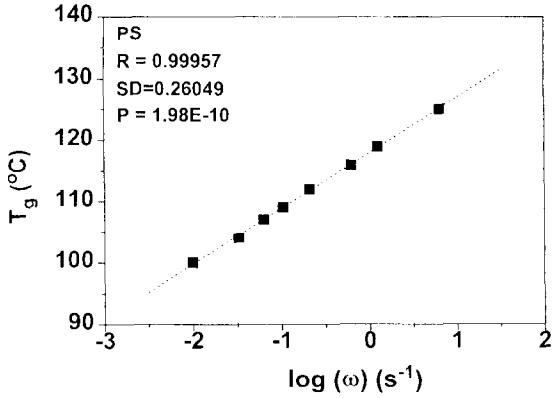

Fig. 3. Theoretical T_g versus frequency for polystyrene.

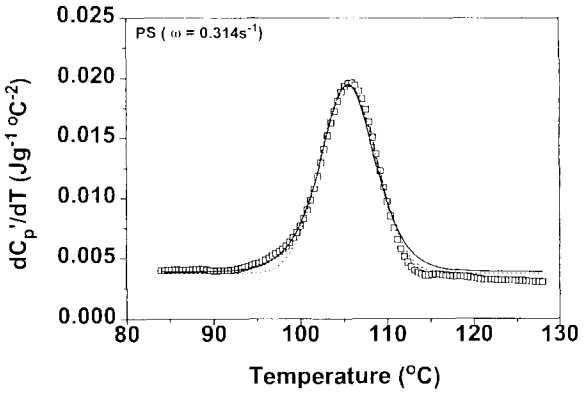

Fig. 4. Comparison of the dC_p'/dT vs. temperature data for theoretical (solid line), experimental (square points) and a Gaussian function (dots) for polystyrene.

$A = 0.8\ \mathrm{J\ g^{-1}{}^{\circ}C^{-1}}$ (assumed value); $B = 0.002\ \mathrm{J\ g^{-1}{}^{\circ}C^{-2}}$ (assumed value) and $\tau_g = 100$ s (from [10]).

Figs. 4 and 5 give the comparison of the dC_p'/dT vs. temperature data for experimental (square points), theoretical (solid line) and a Gaussian function (dots) for polystyrene and a 50/50 by weight blend of poly(methyl methacrylate) and poly(styrene-coacrylonitrile) (50/50) [14]. Obviously, the experimental data can be described by theory, and also well by a Gaussian function at the glass transition. For simplicity, in this paper, we use a Gaussian function to describe the variation of dC_p'/dT vs. temperature at the glass transition.

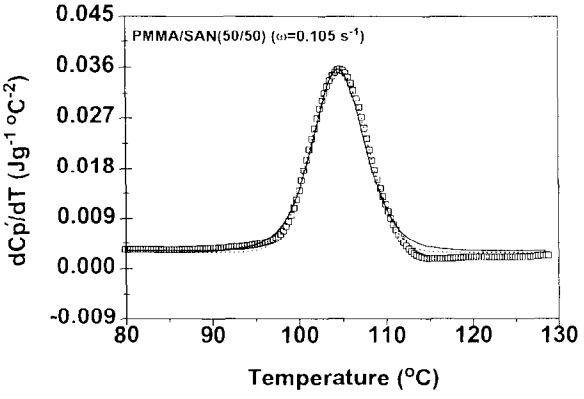

Fig. 5. Comparison of the dC_p'/dT vs. temperature data for theoretical (solid line), experimental (square points) and a Gaussian function (dots) for PMMA/SAN(50/50).

2. Experimental

2.1. IPN sample preparation

The polyurethane component hard segment was composed of the aliphatic diisocyanate 1,1,3,3,-tetramethylxylene diisocyanate (TMXD1) and the chain extender/cross-linker trimethylol propane. The soft segment was made up of polyoxypropylene glycol units of a molar mass of 1025. Stannous octoate was used as the PUR catalyst. The polystyrene was cross-linked with divinylbenzene (DVB) and radical polymerisations were initiated with azoisobutyronitrile (AIBN). The required amount AIBN was added to the TMXDI diisocyanate and the components were mixed for five minutes at high speed. Degassing for 1 min under vacuum was conducted to remove entrapped air. The mixture was cast into stainless steel spring-loaded O-ring moulds, which had been pre-treated with CIL Release 1771 E release agent. The curing cycle consisted of three stages of 24 h at 60°C, 24 h at 80°C and 24 h at 90°C. Symbols used in the study for the PUR/PS IPN series are shown in Table 1.

2.2. Instrumentation

A TA modulated-temperature differential scanning calorimeter was used. An oscillation amplitude of 1.5 and an oscillation of period 60 s were used with a heating rate of 3°C/min. The calorimeter was calibrated with indium and sapphire standards.

Table 1
Symbols for the PUR/PS IPN series

Symbol	PUR/PS	Diol/triol	DVB
IPN1	60/40	7 : 1	5 mol%
IPN2	60/40	3 : 1	5 mol%
IPN3	60/40	1 : 1	5 mol%
IPN4	60/40	3 : 1	5 mol% with 1 wt% of TMI[a]
IPN9	60/40	3 : 1	5 mol% with 2.5 wt% of TMI
IPN5	60/40	3 : 1	5 mol% with 5 wt% of TMI
IPN6	60/40	3 : 1	5 mol% with 10 wt% of TMI
IPN7	60/40	3 : 1	5 mol% standard polymerisation
IPN8	60/40	3 : 1	5 mol% with 10 wt% of compatibiliser[b]

[a] TMI – benzene-1-(1-isocyano-1-methyl ethyl)-3-(2-methylethenyl).
[b] Compatibiliser – a PPE1025 molecule terminated at both ends with TMI units is incorporated in the PS network.

The dynamic mechanical properties of the IPN samples were measured with a Polymer Laboratories MKII Dynamic Mechanical Analyser in the bending mode (single cantilever). The temperature programme was run from −60 to 200°C, using a heating ramp of 3°C/min at a fixed frequency of 10 Hz.

2.3. *Curve synthesis and analysis of overlapping spectral features*

A new signal, the differential of heat capacity, dC_p'/dT, was developed in this work. Fig. 6 gives an example for the change of dC_p'/dT (square points) with temperature for IPN7. Obviously, the signal in glass-transition region is quite complex. Analysing the signal needs curve synthesis and multi-peak resolution techniques.

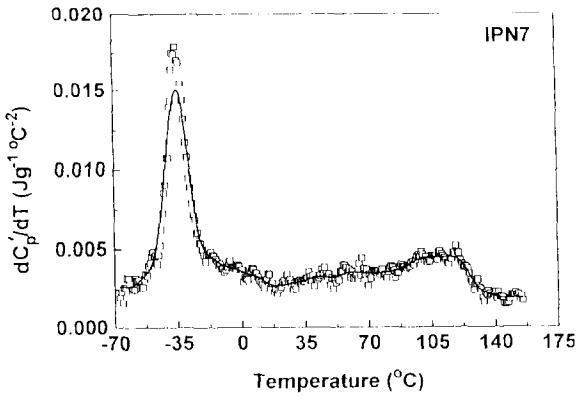

Fig. 6. Untreated dC_p'/dT and smoothed dC_p'/dT vs. temperature data for IPN7.

Nearly all data systems provide a facility to smooth the data. Such an operation must be carried out with care and this section is concerned with the effect that smoothing has upon data and suggests how smoothing might be carried out in the most effective and least distorting way. In general, it is always much better to use unsmoothed data, since any smoothing procedure is bound to introduce some sort of distortion to the curve. However, when the dC_p'/dT signal is used, there is significant noise. There are many cases where some smoothing is required. Smoothing is a process that attempts to increase the correlation between points while suppressing uncorrelated noise. Smoothing is achieved by convolution of data with a suitable smoothing function in an appropriate way. The least-squares central point techniques proposed by Savisky and Golay [15] were used in this work. Fig. 6 (solid line) shows how the method can be successfully applied to typical dC_p'/dT data for a multi-component polymer system (IPN 7). Compared with the raw data, the smoothed spectrum contains no new information. The smoothed curve makes some curve features more evident and so is more useful than the unsmoothed spectrum.

3. Results and discussion

3.1. *Model*

The real part of the heat capacity of polymers in the glass transition region can be considered as follows:

$$C_p' = A + BT + F(T) \tag{21}$$

A and B are constants and $F(T)$ is a function of temperature. Outside the transition region, $F(T) = 0$. For dC_p'/dT, the following relation holds.

$$dC_p'/dT = B + dF(T)/dT = B + f(T) \tag{22}$$

Dotted curves shown in Figs. 4 and 5 can be described by a Gaussian function:

$$f(T) = \Delta C_p/[\omega_d(\pi/2)^{1/2}]\exp[-2(T - T_g)^2/\omega_d^2] \tag{23}$$

where ω_d is the half width of the Gaussian function.

For a multi-phase system, we consider $f(T)$ as a multiple Gaussian function in the transition region:

$$f(T) \equiv \sum_i f_i(T, T_{gi}, \omega_{di}, \Delta C_{pi})$$
$$= \Delta C_{p1}/[\omega_{d1}(\pi/2)^{1/2}]\exp[-2(T - T_{g1})^2/\omega_{d1}^2] + \Delta C_{p2}/[\omega_{d2}(\pi/2)^{1/2}] \times \exp[-2(T - T_{g2})^2/\omega_{d2}^2] + \Delta C_{p3}/[\omega_{d3}(\pi/2)^{1/2}] \times \exp[-2(T - T_{g3})^2/\omega_{d3}^2] + \ldots. \quad (24)$$

where $f_i(T)$ is related to the ith phase of the multi-phase system.

For a multi-phase polymeric system, the total ΔC_p is the linear addition of ΔC_{pi} of each phase [14].

$$\Delta C_p = \sum_i \Delta C_{pi} \quad (25)$$

For a multi-phase system of two polymers, consider the polymer 1-rich phase. Its glass-transition temperature, $T_g^{(1)}$, and increment of heat capacity, $\Delta C_p^{(1)}$, are as follows:

$$T_g^{(1)} = w_1^{(10)} T_{g1} + w_2^{(10)} T_{g2}$$
$$\Delta C_p^{(10)} = w_1^{(10)} \Delta C_{p1} + w_2^{(20)} \Delta C_{p2}$$

Then, the weight fraction of polymer 1-rich phase, $w^{(1)}$, is given by Eq. (26)

$$w^{(1)} = \Delta C_p^{(1)}/\Delta C_p^{(10)} \quad (26)$$

where $w_1^{(10)}$ and $w_2^{(10)}$ are the weight fractions of polymer 1 and polymer 2, respectively, in the polymer 1-rich phase, assuming they are fully miscible. $\Delta C_p^{(10)}$ is the heat capacity increment of polymer 1-rich phase, also assuming full miscibility. From Eq. (27), the weight fractions of other phases can be obtained:

$$w_i = \Delta C_p^{(i)}/\Delta C_p^{(i0)} \quad (27)$$

To evaluate the model, a four-phase model system was devised. This system was a mixture of poly(methyl acrylate)/poly(vinyl acetate) (PMA/PVAc) blends. A PMA/PVAc (80/20)+PMA/PVAc (60/40) +PMA/PVAc (40/60) +PMA/PVAc (20/80, wt/wt) combination was used. PMA is miscible with PVAc [16]. The open square points shown in Fig. 7 represent the change of experimental dC_p'/dT, plotted against temperature. The difference between

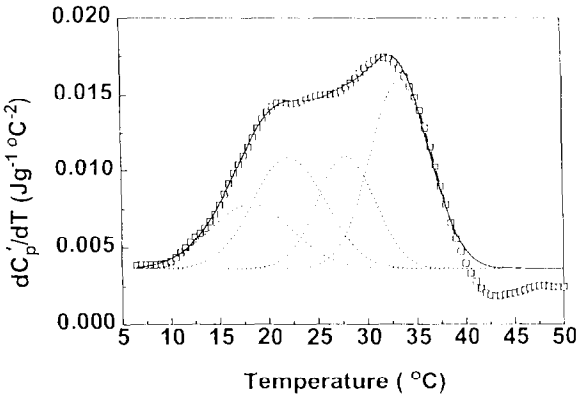

Fig. 7. Comparison of experimental data with peak-resolution results for a four-component physical blend of PMA/PVAc (80/20) +PMA/PVAc (60/40)+PMA/PVAc (40/60)+PMA/PVAc (20/80).

Table 2
Comparison of experimental with calculated compositions[a]

System	Experimental (wt%)	Calculated (wt%)
PMA-20	30	27.8
PMA-40	23	21.1
PMA-60	25	22.9
PMA-80	22	19.7

[a] Average error is about 8%.

the glass-transition temperatures of PMA and PVAc is about 35°C. The glass-transition signal of the four-phase system shows an overlapping transition peak. The solid lines shown in Fig. 7 are peak resolution results. The conditions for peak resolution are as follows.

$$1: \Delta C_p(\text{fitting}) = \Delta C_p(\text{experimental})$$
$$2: \Delta T_g = w_1 \Delta T_{g1} + w_2 \Delta T_{g2}$$

Here, ΔT_g is the transition width and ΔT_{g1} and ΔT_{g2} are the glass-transition widths of pure polymer 1 and polymer 2, respectively.

Table 2 gives the comparison of the results for the experiment by weighing and by calculation. The average error is about 8%.

3.2. Glass-transition behaviour of the IPNs

Almost all IPNs are multi-phase materials. This results in a complicated glass-transition behaviour

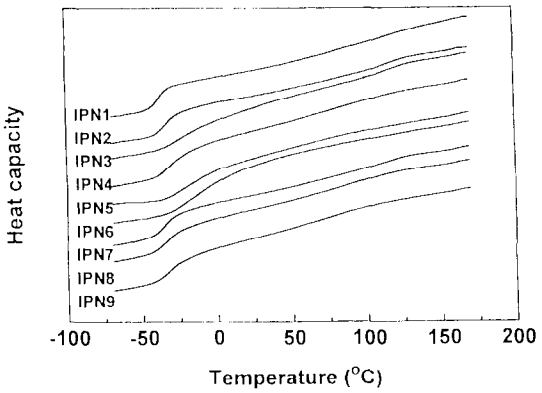

Fig. 8. Heat capacity vs. temperature for IPN1, IPN2, IPN3, IPN4, IPN5, IPN6, IPN8 and IPN9.

[17]. Fig. 8 shows that the heat capacities change with temperature for IPN1 to IPN9.

Fig. 9((1)–(7)) show the changes of the differential of heat capacity, dC_p'/dT, with temperature for IPN1, IPN2, IPN4, IPN5, IPN6, IPN8 and IPN9. Obviously, it is hard to obtain detailed information from the heat capacity signals in Fig. 8. However, the dC_p'/dT signal is very different, being much more sensitive to the transition. The dC_p'/dT vs. temperature signals for these IPNs show obvious nonlinear changes between the T_{gs} of two pure network polymers.

Fig. 10 shows a comparison of the dC_p'/dT vs. temperature plots for a 40% PS+60% PUR physical blend (solid line) and IPN3. It is obvious from this figure that the morphologies of these IPN samples are quite complex. The transition regions are very broad. The total temperature range covered by the transitions is ca. 180°C, covering the transition regions of both pure PUR and PS.

At ca. −36, 70 and 110°C, there are three obvious transitions for IPN1 and IPN2. There are two transitions, for IPN3 at ca. −25 and 110°C. There is also a broad shoulder on the high-temperature side of the lower transition for this sample. In these IPNs, the PUR network is being tightened by altering the diol/triol ratio. The transitions at ca. −36, 70 and 100°C correspond to the soft and the hard segment transitions of the PUR and to the PS glass transition. The shift and broadening in these IPNs are consistent with increasing cross-linking in the PUR component. (See Table 3 for further details).

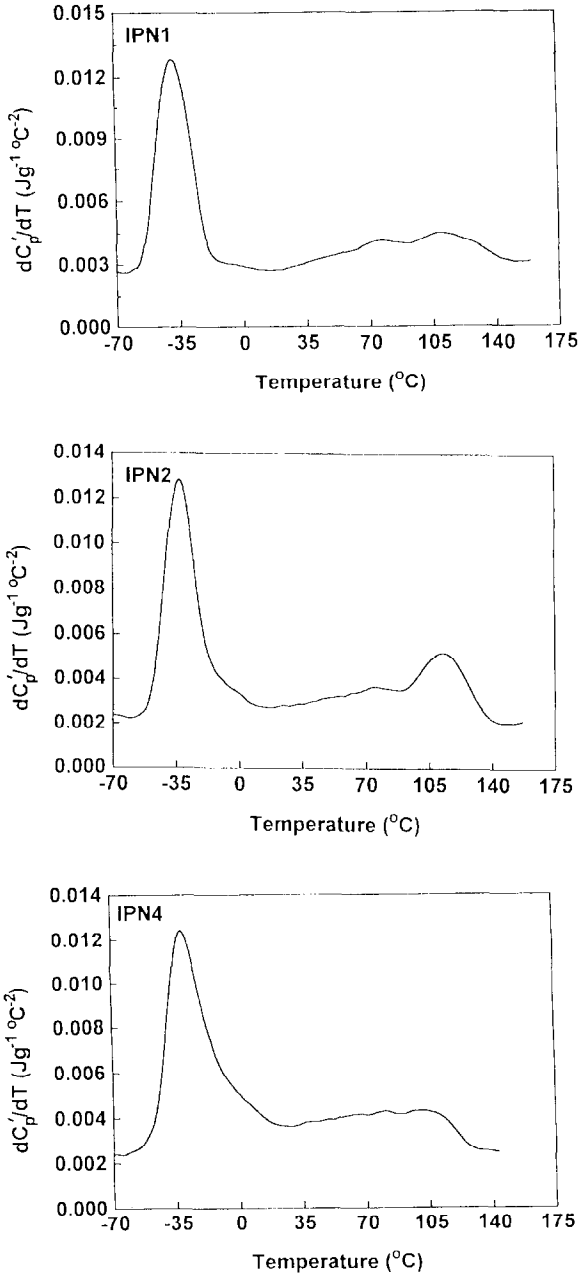

Fig. 9. dC_p'/dT vs. temperature plots for IPN1, IPN2, IPN4, IPN5, IPN6, IPN8 and IPN9.

In IPN4, IPN5, IPN6 and IPN9, TMI has been incorporated into the PUR network as grafting sites for the PS networks. As has been found with IPNs,

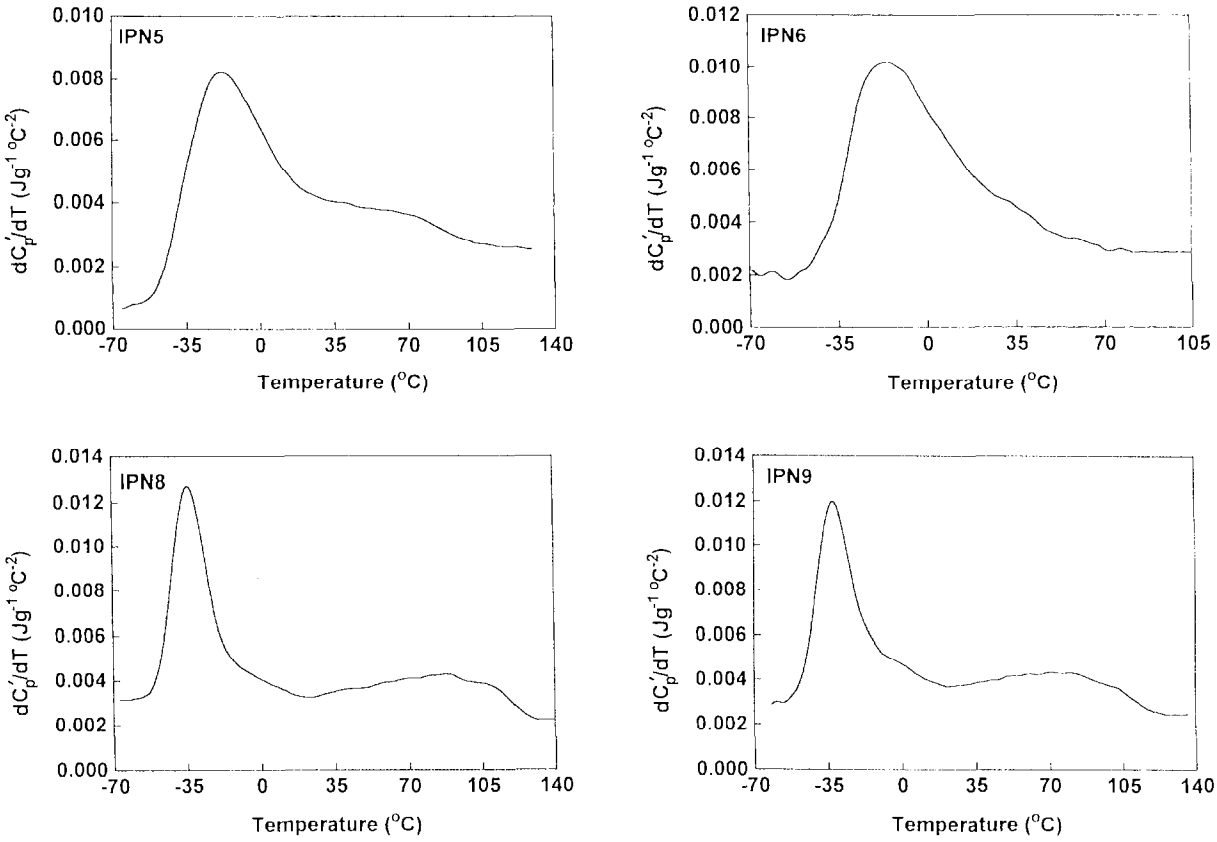

Fig. 9. (Continued)

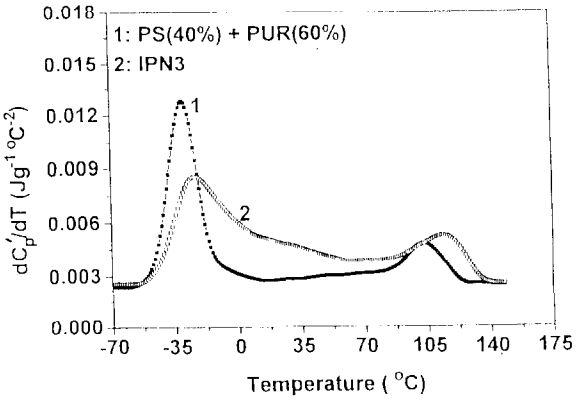

Fig. 10. dC_p'/dT vs. temperature plots for a 40% PS+60% PUR physical blend and for IPN3.

increasing inter-network grafting leads to eventual miscibility. This is seen in a single transition for IPN6, which contains 10 wt% TMI.

Table 3
Cross-linking variations and glass-transition temperatures

Diol/triol	DVB	T_g(°C)	
		PU-rich phase	PS-rich phase*
7 : 1 (IPN1)	5%	−38	113
3 : 1 (IPN2)	5%	−33	113
1 : 1 (IPN3)	5%	−24	113

The effect of the variation of the cross-link level in the PUR has also been studied by DMTA for IPN1, IPN2 and IPN3. Data are shown in Fig. 11. With increasing PUR cross-linking, the PUR transition broadens and the PS transition remains at the same location. This is in agreement with the M-TDSC results.

IPN8 has polypropylene glycol units incorporated into the PS network in an attempt to generate partial

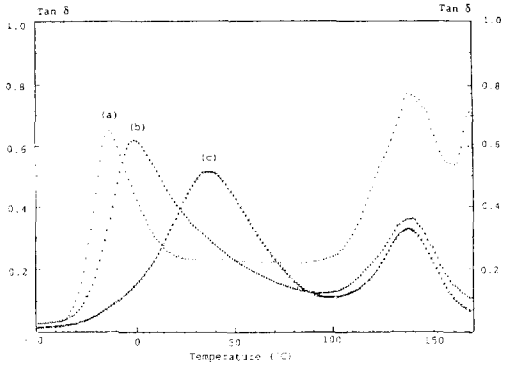

Fig. 11. DMTA data for different PUR network cross-link levels: (a) – IPN1; (b) – IPN2; and (c) – IPN3.

miscibility. Comparison with IPN2 indicates that the PUR hard segment transition is no longer obvious, indicating that the strategy may have been partly successful.

These simultaneous PUR/PS IPNs were synthesised by the one-shot route. The IPN topology can restrict phase separation and result in materials with a broad transition region. By variation of the cross-link level in both polymer networks, the controlled introduction of inter-network grafting and the incorporation of compatibilising segments into the PS network, the compatibility of two polymer networks was improved.

With simultaneous IPNs, it was found [18] that the network that is first formed represents the continuous phase. Hourston and Schäfer [19] investigated the rate of network formation of IPN7 by means of FT-IR spectroscopy using a Unicam spectrometer coupled with a heated cell unit. The conversion curves of both networks were monitored by following integrated peak areas against time. The integration limits for the respective functional groups were (2330–2160) cm^{-1} for the isocyanate and (1637–1622) cm^{-1} for the vinyl group. This study confirmed that under the present reaction conditions, the PUR network was formed first. In such a situation, it is believed that three possible morphologies could result: (a) the two networks could be miscible, yielding homogeneous materials; (b) the first-formed network is uniformly distributed in space, but the second-formed network is heterogeneously distributed; and (c) both networks could be heterogeneously distributed in space, but with an interfacial zone containing a mixture of the two networks. Obviously, for the first situation, a single glass-transition temperature would be obtained. For the second situation, the glass-transition temperature of the PUR will shift to higher temperatures and the PS T_g will shift to lower temperatures. For the third situation, the glass-transition temperature will broaden.

The dC'_p/dT signal shows nonlinear change over a broad temperature range between the glass transitions of PUR and PS. Obviously, these M-TDSC results indicated the third situation. This implies that, during synthesis, a phase separation occurs and an interpenetrating morphology is formed.

3.3. *Phase structure and weight fraction*

IPNs comprise two components of different synthetic origin; one of step growth and the other by radical polymerisation. These two components form several kinds of separated domains, which have different segment concentration distributions at the microstructural level. We can consider that this system can be divided into several phases: polymer 1-rich(1), polymer 2-rich(1), polymer 1-rich(2), polymer 2-rich(2) and interfacial phases and so on. It is difficult to separate the polymer-rich and interfacial phases for these samples. So, we have to consider the interface in these IPNs as a phase which has an average concentration. Fig. 12((1)–(5)) show the peak resolution results for IPN1, IPN2, IPN6, IPN8 and IPN9. The open square points are the experimental ones. Fig. 13 gives a comparison of the dC'_p/dT vs. temperature plots for the 40% PS+60% PUR physical blend and peak resolution for IPN3. For IPN1, three transition peaks were obtained with a three-phase structure. For IPN2, IPN3, IPN8 and IPN9, four transition peaks were obtained with a four-phase structure.

DMTA measurements showed that the glass-transition temperature of the PS-rich phase in the IPN1, IPN2 and IPN3 were the same, 133°C. However, M-TDSC raw data for the same three IPNs showed that the glass-transition temperature of the PS-rich phases were different. However, peak resolution gives the same glass-transition temperature value, again 113°C for the PS-rich phase in IPN1, IPN2 and IPN3. The

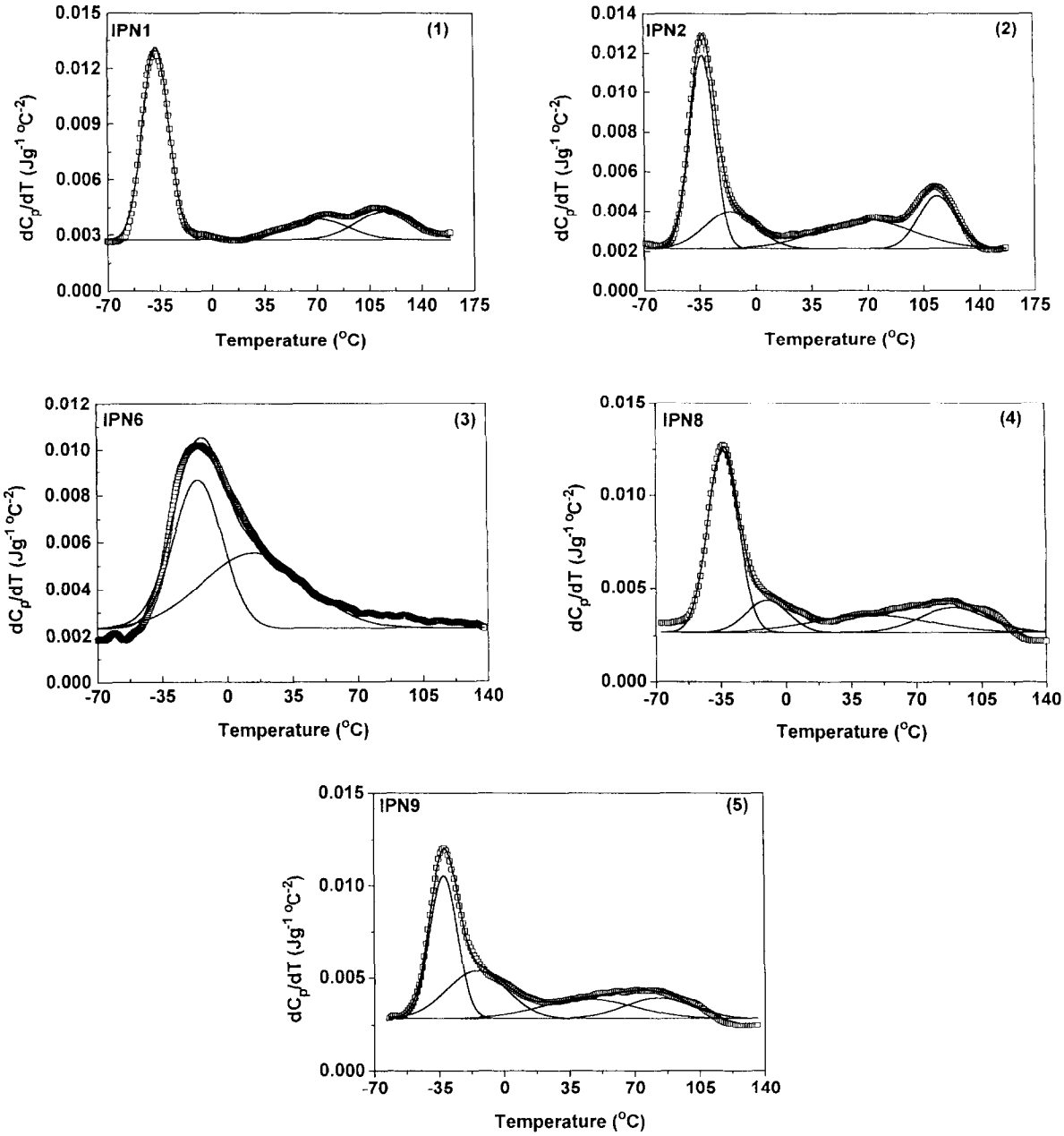

Fig. 12. Comparison of experimental data with peak-resolution results for IPN1, IPN2, IPN6, IPN8 and IPN9.

difference may result from the effect of interface which results in the shift of the dC_p'/dT peak. Table 4 gives the peak resolution results for IPN1, IPN2, IPN3, IPN8 and IPN9.

4. Conclusions

The dC_p'/dT vs. temperature signal from M-TDSC can be used to study morphology of IPNs. The transi-

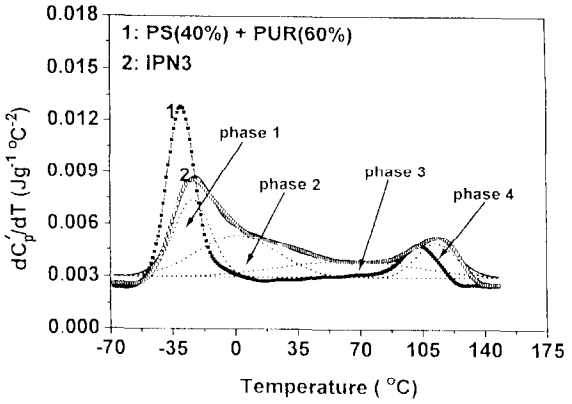

Fig. 13. Comparison of experimental data for the 40% PS+60% PUR physical blend and peak resolution results for IPN3.

Table 4
Phase T_g and weight fraction for selected IPNs

	T_g(°C)	Weight fraction (%)
IPN1	−37	59
	70	14
	113	30
IPN2	−35	48
	−15	16
	70	15
	113	20
IPN3	−23	19
	−15	30
	75	31
	113	16
IPN8	−33	45
	−10	14
	46	21
	90	19
IPN9	−33	32
	−17	23
	50	30
	90	19

tion function is a Gaussian function of temperature in glass-transition region for polymers. These parameters in the transition function have clear physical meaning. The transition function of multi-phase polymeric systems is the linear sum of the transition function of each phase:

$$f(T) \equiv \sum_i f_i(T, T_{gi}, \omega_{di}, \Delta C_{pi})$$
$$= \Delta C_{p1}/[\omega_{d1}(\pi/2)^{1/2}] \times \exp[-2(T - T_{g1})^2/\omega_{d1}^2] + \Delta C_{p2}/[\omega_{d2}(\pi/2)^{1/2}] \times \exp[-2(T - T_{g2})^2/\omega_{d2}^2] + \Delta C_{p3}/[\omega_{d3}(\pi/2)^{1/2}] \times \exp[-2(T - T_{g3})^2/\omega_{d3}^2] + \ldots.$$

The transition function can be used to fit experimental results and calculate the number of phases present, the weight fraction and the transition temperature of each phase. A model experiment showed that the error in calculating the weight fraction of each phase is ca. 8%. As examples of the application of this new mode of analysis, polystyrene/polyurethane IPNs were analysed.

References

[1] A.S. Vaughan, Polymer microscopy, in B.J. Hunt and M.I. James (Eds.), Polymer Characterisation, Blackie Academic & Professional, London, 1993.
[2] M. Shibayama and T. Hashimoto, Macromolecules, 19 (1986) 740.
[3] T. Hashimoto, K. Nagatoshi, A. Todo, H. Hasegawa and H. Kawai, Macromolecules, 7 (1974) 364.
[4] C.G. Vonk, J. Appl. Crystallogr., 6 (1973) 81.
[5] U. Siemann and W. Ruland, Colloid Polym. Sci., 260 (1982) 999.
[6] T. Hashimoto, M. Fujimara and H. Kawai, Macromolecules, 13 (1980) 1660.
[7] R.J. Roe, J. Appl. Crystallogr., 15 (1982) 182.
[8] W. Ruland, Macromolecules, 20 (1987) 87.
[9] F. Annighofer and W. Gronski, Colloid Polym. Sci., 261 (1983) 15.
[10] A.J. Covacs and J.M. Hutchinson, J. Polym. Sci. Polym. Phys., 14 (1976) 1575.
[11] M. Reading, Trends in Polymer Science, 2 (1993) 248.
[12] A.A. Lacey, C. Nikolopoulos, H.M. Pollock and M. Reading, submitted to J. Thermol. Analysis, 1996.
[13] M. Reading, R. Wilson and H.M. Pollock, Proceedings of the 23rd North American Thermal Analysis Scociety Conference, 1994, pp. 2–10.
[14] M. Song, H. Ammiche, H.M. Pollock, D.J. Hourston and M. Reading, Polymer, 36 (1995) 3343.
[15] A. Savisky and M.J.E. Golay, Anal. Chem., 36 (1964) 1627.

[16] A.K. Nandi, B.M. Mandal and C. Bhattacharyya, Macromolecules, 18 (1985) 1454.
[17] L.H. Sperling, Interpenetrating Polymer Networks, Plenum Press, New York, 1981.
[18] A.A. Ponatelli, L.H. Sperling and D.A. Thomas, J. Appl. Polym. Sci., 21 (1977) 1189.
[19] D.J. Hourston and F.U. Schäfer, J. Polym. Adv. Technol., 7 (1995) 273.